Simplified Kinetic Model for NH3-SCR Over Cu-CHA Based on First-Principles Calculations

Citation for the original published paper (version of record):
Feng, Y., Creaser, D., Grönbeck, H. (2023). Simplified Kinetic Model for NH3-SCR Over Cu-CHA Based on First-Principles Calculations. Topics in Catalysis, 66(13-14): 743-749.
http://dx.doi.org/10.1007/s11244-022-01711-5

Topics in Catalysis
https://doi.org/10.1007/s11244-022-01711-5

ORIGINAL PAPER

Simplified Kinetic Model for NH_3-SCR Over Cu-CHA Based on First-Principles Calculations

Yingxin Feng[1] · Derek Creaser[2] · Henrik Grönbeck[1]

Accepted: 30 September 2022

Abstract

Selective catalytic reduction with ammonia as reducing agent (NH_3-SCR) is an efficient technology to control NO_x emission during oxygen excess. Catalysts based on Cu-chabazite (Cu-CHA) have shown good performance for NH_3-SCR with high activity and selectivity at low temperature and good hydrothermal stability. Here, we explore a first-principles based kinetic model to analyze in detail which reaction steps that control the selectivity for N_2 and the light-off temperature. Moreover, a simplified kinetic model is developed by fitting lumped kinetic parameters to the full model. The simplified model describes the reaction with high accuracy using only five reaction steps. The present work provides insight into the governing reaction mechanism and stimulates design of knowledge-based Cu-CHA catalysts for NH_3-SCR.

Keywords First-principles microkinetic modeling · NH_3-SCR · Cu-CHA · Parameter evaluation

1 Introduction

Copper-exchanged small-pore zeolites with chabazite structure (Cu-CHA), are state-of-the-art catalysts for ammonia assisted selective catalytic reduction (NH_3-SCR) in emission control of diesel exhaust [1]. Thanks to low-temperature activity, high selectivity for N_2, and hydrothermal stability [2–4], Cu-CHA is a preferred catalyst for NH_3-SCR and has matured to commercial application. NO is the main NO_x component in diesel exhaust and selective reduction of NO to N_2 with NH_3 is known as the standard-SCR reaction:

$$4NH_3 + 4NO + O_2 \rightarrow 4N_2 + 6H_2O \quad \text{(R1)}$$

Each NO couples with one NH_3 and O_2 is needed to complete the stoichiometry.

Although high selectivity for N_2 has been achieved over Cu-CHA, a small amount of N_2O is formed under NH_3-SCR conditions [5, 6]. N_2O is an undesired by-product and has received wide attention due to its high greenhouse protential. An overall reaction where N_2O is formed is:

$$2\,NH_3 + 2\,NO + O_2 \rightarrow N_2 + N_2O + 3\,H_2O \quad \text{(R2)}$$

To further enhance the selectivity for N_2 over Cu-CHA, understanding of the reaction mechanism for N_2O formation during NH_3-SCR is desired. Advancing the atomic understanding of the reactions could in this respect guide the development of next generations of catalysts. For this purpose we have developed first-principles microkinetic models for low-temperature conditions [7] based on multi-site reaction mechanisms [8].

The proposed reaction cycle for NH_3-SCR is shown in Fig. 1. Under the reaction condition of standard NH_3-SCR, Cu ions are at low temperatures solvated by NH_3 and mainly present as $[Cu(NH_3)_2]^+$ species [9–11]. O_2 adsorption is a key step in the reaction and a pair of $[Cu(NH_3)_2]^+$ complexes is needed for O_2 adsorption, forming a Cu-peroxo complex, $[Cu_2(NH_3)_4O_2]^{2+}$ [9, 12, 13]. The oxidation state of Cu changes from +1 to +2 [14] during O_2 adsorption, which allows the adsorption of NO and NH_3 at relevant temperatures. Upon NO adsorption (reaction 2), NO reduction

---

✉ Yingxin Feng
yingxin@chalmers.se

✉ Henrik Grönbeck
ghj@chalmers.se

Derek Creaser
derek.creaser@chalmers.se

[1] Department of Physics and Competence Centre for Catalysis, Chalmers University of Technology, 41296 Göteborg, Sweden

[2] Department of Chemistry and Chemical Engineering, Chalmers University of Technology, 41296 Göteborg, Sweden

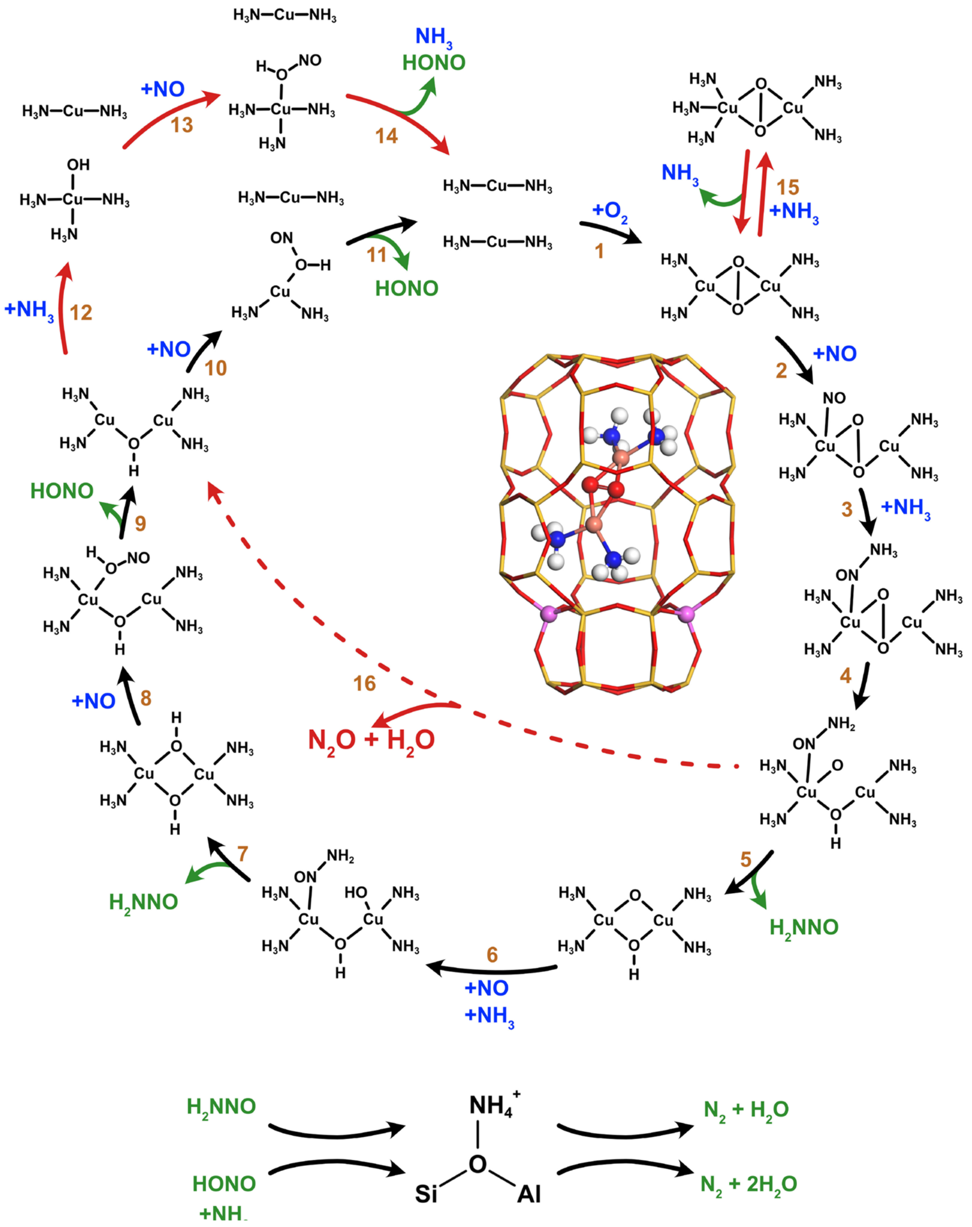

Fig. 1 Proposed reaction cycle for low-temperature NH_3-SCR over Cu-CHA and the side view of the chabazite cages showing the Al positions in the six-membered ring which also includes the $[Cu_2(NH_3)_4(O_2)]^{2+}$ complex. Atom color codes: Cu (bronze), Si (yellow), Al (pink), O (red), N (blue), and H (white). Adapted from Ref. [7]

proceeds via formation of H_2NNO and HONO intermediates. The intermediates is in this model assumed to diffuse from the Cu-sites to neighboring Brønsted acid sites where they decompose into N_2 and H_2O by reactions with NH_3 [7, 8]. Unwanted N_2O formation (reaction 16) may occur via H_2NNO decomposition over the Cu-sites [7, 15]. The selectivity for N_2 depends on the competition between the diffusion of H_2NNO from the $[Cu_2(NH_3)_4OOH]^{2+}$ complex to the Brønsted acid sites (reaction 5) and the direct decomposition of H_2NNO on the complex (reaction 16). If H_2NNO desorbs from the Cu complex, the reaction will follow the outer cycle and give an overall reaction as R1. However, for the case that H_2NNO decomposes over the Cu complex, the reaction will follow the dashed route which forms N_2O as R2.

NO conversion to either N_2 or N_2O may be inhibited by NH_3 adsorption on the $[Cu_2(NH_3)_4O_2]^{2+}$ complex (reaction 15). The NH_3 adsorption is in the reaction cycle yielding $[Cu_2(NH_3)_5O_2]^{2+}$, however, it may also lead to decomposition of the peroxo complex [7, 13]. Note that NH_3 has four different roles in the catalytic cycle showed in 1. NH_3 is simultaneously i) a ligand that enable facile Cu-mobility, ii) a reactant, iii) adsorbed at the Brønsted acid site forming NH_4^+, which is the active site for H_2NNO and HONO conversion, and iv) an inhibitor that prevents the adsorption of NO on the Cu-peroxo complex [7].

In this contribution, we further investigate factors that control the selectivity for N_2 and the NH_3 inhibition. For the selectivity for N_2, the competition between reaction 5 and

16 is discussed in detail. It is revealed that a reduction of the H_2NNO desorption energy on the Cu-peroxo enhances the selectivity for N_2, which is one possibility to further improve the catalyst performance. The NH_3 inhibition is discussed in relation to the onset of the low-temperature activity and different mechanisms to exit the blocked state are presented. In addition to the mechanistic aspects, we show that the detailed microkinetic model with 18 steps can be replaced with a simplified model with only 5 steps, which accurately reproduce the results of the full model.

2 Computational Methods

2.1 Density Functional Theory Calculations

Spin-polarized density functional theory (DFT) calculations are carried out with the Vienna Ab-initio Simulation Package (VASP) [16–19], using the gradient-corrected Perdew-Burke-Ernzerhof (PBE) functional [20] augmented with a Hubbard-U term of 6 eV for the Cu 3d states as proposed in previous studies [21, 22]. To account for the van der Waals interactions of the molecules in the zeolites, Grimme-D3 corrections have been applied [23, 24]. The valence electrons are described with a plane wave basis set with a cutoff energy of 480 eV, whereas the interaction between the valence and the cores are described using the projector augmented wave (PAW) method [25, 26]. The k-point sampling is restricted to the gamma point. The Climbing Image Nudged Elastic Band (CI-NEB) method [27, 28] is employed to calculate the reaction barriers and the transition states are confirmed by vibrational analyses. *Ab initio* molecular dynamics (AIMD) simulations are performed in the canonical (NVT) ensemble [29, 30] at 300 K to probe the potential energy surface and low energy configurations are obtained by structural relaxation from the trajectories. The experimental lattice constants ($\alpha = \beta = \gamma = 94.2°$, $a = b = c = 9.42$ Å) are used for the CHA unit cell.

2.2 Microkinetic Modeling

For the microkinetic modeling, MATLAB R2018b is used with the `ode23s` solver to numerically integrate the system of differential equations until steady-state is reached. The full model includes 16 reaction steps as shown in Fig. 1 and two steps over the Brønsted acid sites [7]. The kinetic parameters for the full model are published elsewhere [7].

Here, a simplified model with only five reaction steps is developed. The simplified model uses lumped reaction steps with kinetic parameters estimated by fitting to the detailed model. The `simulannealbnd` optimizer is applied to perform the non-linear regression. An objective function (τ) for the parameter estimation is chosen as the normalized difference between the results from the detailed model (denoted ref) and the simplified model (denoted sim):

$$\tau = \sum_T \left(\sqrt{\left(\frac{\mathrm{TOF_{sim}}}{\mathrm{TOF_{ref}}} - 1 \right)^2} + w\sqrt{\left(\frac{\mathrm{S_{sim}}}{\mathrm{S_{ref}}} - 1 \right)^2} \right) \qquad (1)$$

where the turnover frequency of NO and selectivity for N_2 are denoted TOF and S, respectively. A weighting factor (w = 10) is added to the part of the normalized difference in selectivity to enhance the importance of the selectivity.

3 Results and Discussion

3.1 Steps Controlling the Selectivity and Light-Off Temperature

Here we further investigate the steps that previously [7] were found to determine the selectivity for N_2 and the light-off temperature for NH_3-SCR over Cu-CHA. The aim is to gain deeper insights into the mechanisms that control these steps and reveal how they influence the kinetic behavior.

3.1.1 Selectivity for N_2

In the kinetic model [7], the selectivity for N_2 depends on the ratio between reaction rate of reaction 5 and reaction 16. Reaction 5 contains desorption of H_2NNO from $[Cu_2(NH_3)_4OOH]^{2+}$ and diffusion through an eight membered ring in the zeolite to a Brønsted acid site. Previous calculations show that H_2NNO desorption is associated with a barrier of 0.3 eV and that the barrier for diffusion is about 0.1 eV. The effective barrier for reaction 5 is, thus, set to 0.3 eV. For reaction 16, the decomposition of H_2NNO over $[Cu_2(NH_3)_4OOH]^{2+}$ forming N_2O, H_2O and $[Cu_2(NH_3)_4OH]^{2+}$ may involve changes in the spin configuration [15], which makes it challenging to determine accurately the reaction barrier. Here we have considered the case where the spin state of the Cu-cations are preserved along the reaction path.

To investigate how the selectivity depends on the ratio between the barrier of reaction 5 and 16, we performed simulations where the ratio was changed, Fig. 2. In the simulations, the forward reaction barrier of Reaction 5 (E_{5f}) was fixed to 0.3 eV, whereas the forward reaction barrier of reaction 16 (E_{16f}) was changed from 0.3 to 0.42 eV.

The selectivity for N_2 depends strongly on the E_{16f}/E_{5f} ratio at low ratios. The selectivity at 373 K increase from 80% to 95% when the ratio increase from 1 to 1.2. The dependence is less pronounced at higher E_{16f}/E_{5f} ratios and the effect of increasing the ratio on the selectivity becomes small for cases when the ratio is larger than 1.3. E_{16f} is close to the calculated DFT barrier when the ratio is 1.3. The

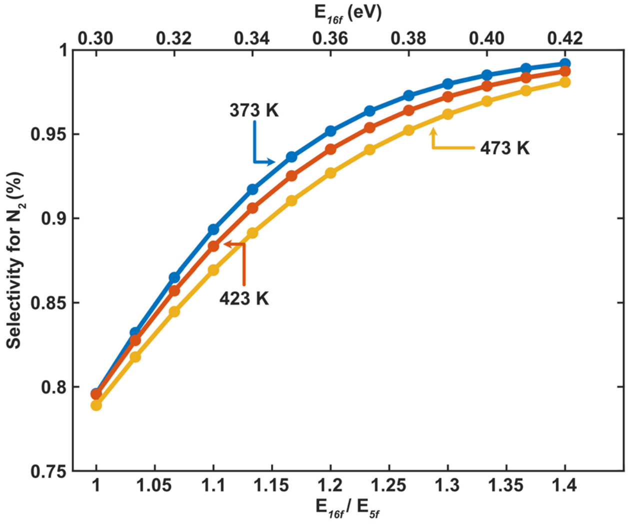

Fig. 2 The selectivity for N_2 for different ratios between the barrier of reaction 5 and reaction 16 at 373, 423, and 473 K, respectively

strong dependence of the selectivity on the E_{16f}/E_{5f} ratio shows that lowering the H_2NNO desorption energy could lead to a higher selectivity for N_2. The desorption energy could potentially be effected by the Al-distribution [31].

3.1.2 Site Blocking and Light-Off Temperature

Adsorption of NH_3 instead of NO on the $[Cu_2(NH_3)_4(O_2)]^{2+}$ complex blocks the site for the SCR-reaction [7]. The inhibiting effect of NH_3 is severe as the adsorption energy of NH_3 is higher than that of NO; -0.98 eV as compared to -0.70 eV. It was in Ref. [7] shown that the light-off temperature of the SCR reaction is determined by the NH_3 inhibition as the temperature should be high enough to facilitate NH_3 desorption. Adsorption of NH_3 on $[Cu_2(NH_3)_4(O_2)]^{2+}$ has also been observed experimentally using X-ray absorption spectroscopy (XAS) [13] where it was suggested that the $[Cu_2(NH_3)_5O_2]^{2+}$ complex dissociates into two Cu complexes $[Cu(NH_3)_3O_2]^+$ and $[Cu(NH_3)_2]^+$. The energy difference between $[Cu_2(NH_3)_5(O_2)]^{2+}$ and $[Cu(NH_3)_3(O_2)]^+$ with $[Cu(NH_3)_2]^+$ was in Ref. [7] calculated to be only 0.04 eV. In the kinetic model [7], the NH_3 inhibition step was considered as adsorption onto $[Cu_2(NH_3)_5O_2]^{2+}$ (reaction 15 in Fig. 1).

It could be noted that molecular crystals have been synthesized with the Cu_2O_2 unit coordinated to six nitrogen-based ligands [32], which indicates that adsorption of additional NH_3 could possibly form $[Cu_2(NH_3)_6O_2]^{2+}$ during NH_3 -SCR in CHA. To investigate the effect of NH_3 inhibition in detail, we have here performed DFT calculations for sequential NH_3 adsorption onto the $[Cu_2(NH_3)_4O_2]^{2+}$ complex, Fig. 3. NH_3 can adsorb on the Cu site of $[Cu_2(NH_3)_4O_2]^{2+}$ with an adsorption energy of -0.98 eV as shown in Fig. 3(B).

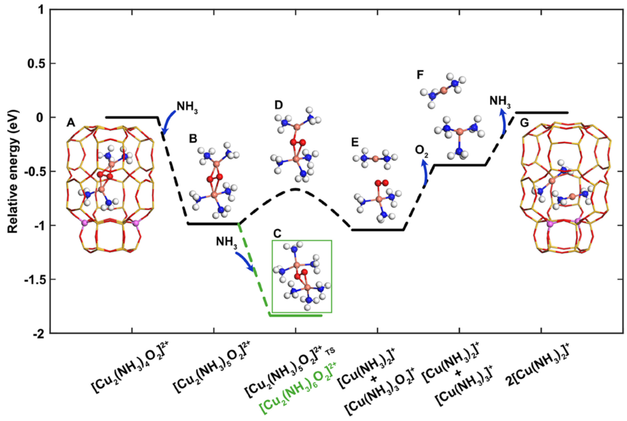

Fig. 3 The potential energy landscape of NH_3 adsorption over $[Cu_2(NH_3)_4O_2]^{2+}$ complex in CHA. Atomic color codes are the same as those in Fig. 1

After forming structure B, an additional NH_3 can adsorb with an adsorption energy of -0.85 eV on the other Cu-cation forming $[Cu_2(NH_3)_6O_2]^{2+}$ (structure C in Fig. 3). Without additional NH_3, structure B could dissociate into structure E via the transition state D. The barrier for dissociation is calculated to be 0.33 eV. Configuration E is consistent with the experimental interpretation of the XAS spectra [13]. As the complex has dissociated, O_2 and NH_3 bonded with the Cu-cation may desorb sequentially with desorption energies of 0.60 eV and 0.49 eV, respectively. The Cu species return in this way to the $[Cu(NH_3)_2]^+$ state on which O_2 may adsorb forming structure A. The adsorption energy of O_2 is here calculated to be only 0.05 eV, which is lower than experiments and previous calculations [33]. The difference can be attributed to differences in the reference state of the initial state for the $[Cu(NH_3)_2]^+$ pairs as well as the poor description of molecular oxygen in the used exchange-correlation functional [34].

The potential energy landscape shows the possible ways of NH_3 hindering the SCR-reaction. The rate of NH_3 adsorption to C is at experimentally relevant conditions lower than the rate for dissociation of B to E, thus, the system will likely transform into E and eventually G. Kinetic analysis (not shown) reveals that this is indeed the case.[1] The kinetic analysis explains why structure C is not observed experimentally despite the strong NH_3 adsorption energy; B will dissociate before NH_3 adsorbs to form C. The system will at temperatures above 423 K mainly be in state G. The probability of being in state A, which is required for the NH_3 -SCR reaction has a maximum at about 473 K.

---

[1] The adsorption energy of O_2 was in the kinetic analysis put to the experimental value of − 0.82 eV. [33]

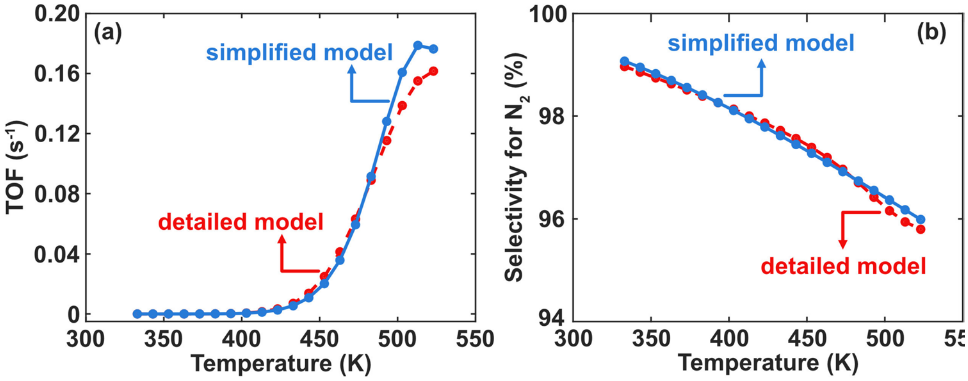

Fig. 4 Simulated turnover frequency for NO conversion (**a**) and selectivity for N_2 (**b**) over Cu-CHA as a function of temperature. The simulations are performed with 600 ppm NH_3, 500 ppm NO, 10% O_2, and balance N_2. The red dashed line in each figure is the results from the detailed model whereas the blue line is from the simplified model

Table 1 Original and estimated parameters for the simplified kinetic model

Reaction	A_f	A_b	ΔE_f	ΔE_b	ΔS_f	ΔS_b
$O_2 + 2* \overset{R3}{\leftrightarrow} *\text{-OO-}*$	–	–	0.13	0.33	– 134.9	17.6
$O_2 + 2* \overset{R3}{\leftrightarrow} *\text{-OO-}*(\text{Exp. }\Delta E)$	8.8×10^4	8.2×10^{13}	0.13	0.95	– 134.9	17.6
$NO + \text{-OO-}* \overset{R4}{\leftrightarrow} NO\text{-OO-}*$	9.7×10^4	9.8×10^{12}	0.00	0.70	– 109.2	0
$NH_3 + *\text{-OO-}* \overset{R5}{\leftrightarrow} NH_3\text{-OO-}*$	2.2×10^4	9.8×10^{12}	0.00	0.98	– 103.8	0
$4NH_3 + 3NO + NO\text{-OO-}* \overset{R6}{\leftrightarrow} 4N_2 + 6H_2O + 2*$	9.3×10^8	–	0.34	14.1	– 14.8	–
$2NH_3 + NO + NO\text{-OO-}* \overset{R7}{\leftrightarrow} N_2 + N_2O + 3H_2O + 2*$	2.4×10^9	–	0.46	10.6	– 7.0	–

Energies are given in eV and entropies in J/mol · K. The pre-exponential factors (A_x) are given in s^{-1} and evaluated at 473 K with 600 ppm NH_3, 500 ppm NO, 10% O_2, and balance N_2

The detailed reaction path for NH_3 inhibition shows that structure E is the dominating structure at low temperatures. For the SCR reaction to proceed, E should decompose allowing for regeneration of structure A. Effectively, however, the inhibition could in a kinetic model be accounted for by considering only structure B as the NH_3 poisoned state.

3.2 Reduced Kinetic Model

In our previous work, the reaction cycle in Fig. 1 was implemented in a kinetic model [7]. The model included 18 elementary steps and it is interesting to investigate whether it could be simplified by lumping reaction steps which do not control the reaction rate. We have shown [7] that the total rate is dominated by the adsorption steps, *i.e.* O_2, NO and NH_3 adsorption onto a pair of $[Cu(NH_3)_2]^+$ complexes. Here we develop a model based on the three adsorption steps and lumped reactions for N_2 and N_2O formation:

$$O_2 + 2* \overset{R3}{\leftrightarrow} *\text{-OO-}* \tag{R3}$$

$$NO + *\text{-OO-}* \overset{R4}{\leftrightarrow} NO\text{-OO-}* \tag{R4}$$

$$NH_3 + *\text{-OO-}* \overset{R5}{\leftrightarrow} NH_3\text{-OO-}* \tag{R5}$$

$$4NH_3 + 3NO + NO\text{-OO-}* \overset{R6}{\leftrightarrow} 4N_2 + 6H_2O + 2* \tag{R6}$$

$$2NH_3 + NO + NO\text{-OO-}* \overset{R7}{\leftrightarrow} N_2 + N_2O + 3H_2O + 2* \tag{R7}$$

The kinetic parameters for the elementary adsorption steps are taken from our previous study [7], whereas the parameters for the lumped reactions (R6 and R7) are determined by fitting to the detailed model. The initial values in the parameter estimation are given by the values corresponding to the highest energy barrier in the lumped reaction. The activation energies and entropy contributions from parameter estimation are listed in Table 1.

The TOF and selectivity from the simplified model is compared to the detailed model in Fig. 4. Both the TOF and selectivity for N_2 are in very good agreement. The onset of the reaction is at about 425 K and is associated with the desorption of NH_3 that blocks the Cu-site. The TOF approaches a maximum at about 525 K as the coverage of O_2 starts to decrease.

Phenomenological models with lumped reaction steps have previously been developed from experimental data for NH_3-SCR over Cu-CHA [35]. In Ref. [35], the pre-exponential factor for the NH_3-SCR reaction was reported to be 4.83×10^8 s^{-1} and the corresponding activation energy to be 0.71 eV. Our model yields a comparable result for the prefactor, which is 9.3×10^8 s^{-1} for the lumped SCR-reaction (R6). However, our activation energy for R6 is 0.34 eV. The difference with respect to the phenomenological model is due to the fact that NH_3-inhibition effectively was included in the SCR-reaction in Ref. [35], whereas it is treated explicitly in our model. In fact, the apparent activation energy of our simplified model is 0.76 eV, which is close to the value used in the phenomenological model. The comparison shows the advantage of a first-principles based model where the kinetic parameters can be associated with elementary reaction steps.

4 Conclusions

We have discussed a first-principles micro-kinetic model for low-temperature NH_3-SCR over Cu-CHA. The model involves formation of H_2NNO and HONO intermediates over $[Cu_2(NH_3)_4O_2]^{2+}$ and diffusion of the intermediates to Brønsted acid sites (NH_4^+) where they decompose to N_2 and H_2O. Unwanted N_2O formation is accounted for by direct H_2NNO decomposition over $[Cu_2(NH_3)_4OOH]^{2+}$. Here, we have analyzed in detail two crucial aspects of the model, namely how the selectivity depends on the ratio between the barriers for H_2NNO diffusion and direct decomposition, and how the SCR-reaction is inhibited by NH_3 adsorption onto $[Cu_2(NH_3)_4O_2]^{2+}$ complex.

The selectivity for N_2 is found to be sensitive to the ratio between the barriers. The barrier for H_2NNO diffusion originates mainly from the desorption from the $[Cu_2(NH_3)_4OOH]^{2+}$ complex and one strategy to enhance the selectivity would be to reduce the desorption energy. The desorption energy could potentially be modified via the Al-distribution.

The micro-kinetic model shows that adsorption of extra NH_3 on $[Cu_2(NH_3)_4O_2]^{2+}$ controls the light-off temperature of the SCR reaction. We show that adsorption of two additional NH_3 forming $[Cu_2(NH_3)_6O_2]^{2+}$ is thermodynamically preferred analogous to crystal structures with the Cu_2O_2 core coordinated to six N-ligands. However, our analysis reveals that decomposition of $[Cu_2(NH_3)_5O_2]^{2+}$ into $[Cu(NH_3)_3O_2]^{+}$ and $[Cu(NH_3)_2]^{+}$ is kinetically preferred at relevant experimental conditions. The formation of $[Cu(NH_3)_3O_2]^{+}$ and $[Cu(NH_3)_2]^{+}$ is in agreement with experimental observations [13]. $[Cu(NH_3)_3O_2]^{+}$ should decompose allowing for the regeneration of the $[Cu_2(NH_3)_4O_2]^{2+}$ complex for the SCR reaction to proceed.

The analysis of the detailed kinetic model allows for the formulation of a simplified model for NH_3-SCR with N_2O formation over Cu-CHA with only five reaction steps. The simplified model was constructed with the elementary reactions for adsorption and desorption of NH_3, NO and O_2 together with lumped reactions for N_2 and N_2O formation. The kinetic parameters for the lumped reactions were fitted via non-linear regression. The simplified model reproduces the results for the detailed model and provides a link to a previous kinetic model developed from experimental data.

Acknowledgements We thank Ton V.W. Janssens, Jonas Jansson and Magnus Skoglundh for discussions and acknowledge financial support from the Swedish Energy Agency (47110-1). The Competence Centre for Catalysis (KCK) is hosted by Chalmers University of Technology and financially supported by the Swedish Energy Agency and the member companies ECAPS, Johnson Matthey, Perstorp, Powercell, Preem, Scania CV, Umicore and Volvo Group. The calculations have been performed at PDC (Stockholm) through a SNIC grant.

Funding Open access funding provided by Chalmers University of Technology.

References

1. Johnson TV (2014) In: Nova I, Tronconi E (eds) Review of selective catalytic reduction (SCR) and related technologies for mobile applications, pp. 3–31. Springer, New York (2014). https://doi.org/10.1007/978-1-4899-8071-7_1
2. Chen H-Y (2014) In: Nova I, Tronconi E (eds) Cu/zeolite SCR catalysts for automotive diesel NOx emission control, pp. 123–147. Springer, New York (2014). https://doi.org/10.1007/978-1-4899-8071-7_5
3. Schmieg SJ, Oh SH, Kim CH, Brown DB, Lee JH, Peden CHF, Kim DH (2012) Thermal durability of Cu-CHA NH_3-SCR catalysts for diesel NO_x reduction. Catal Today 184(1):252–261. https://doi.org/10.1016/j.cattod.2011.10.034
4. Xin Y, Li Q, Zhang Z (2018) Zeolitic materials for $DeNO_x$ selective catalytic reduction. ChemCatChem 10:29–41. https://doi.org/10.1002/cctc.201700854
5. Gao F, Walter ED, Kollar M, Wang Y, Szanyi J, Peden CHF (2014) Understanding ammonia selective catalytic reduction kinetics over Cu/SSZ-13 from motion of the Cu ions. J Catal 319:1–14. https://doi.org/10.1016/j.jcat.2014.08.010
6. Yao D, Liu B, Wu F, Li Y, Hu X, Jin W, Wang X (2021) N_2O formation mechanism during low-temperature NH_3-SCR over

Cu-SSZ-13 catalysts with different Cu loadings. Ind Eng Chem Res 60(28):10083–10093. https://doi.org/10.1021/acs.iecr.1c01514

7. Feng Y, Wang X, Janssens TVW, Vennestrøm PNR, Jansson J, Skoglundh M, Grönbeck H (2021) First-principles microkinetic model for low-temperature NH_3-assisted selective catalytic reduction of NO over Cu-CHA . ACS Catal 14395–14407 https://doi.org/10.1021/acscatal.1c03973
8. Chen L, Janssens TVW, Vennestrøm PNR, Jansson J, Skoglundh M, Grönbeck H (2020) A complete multisite reaction mechanism for low-temperature NH_3-SCR over Cu-CHA. ACS Catal 10(10):5646–5656. https://doi.org/10.1021/acscatal.0c00440
9. Paolucci C, Khurana I, Parekh AA, Li S, Shih AJ, Li H, Di Iorio JR, Albarracin-Caballero JD, Yezerets A, Miller JT et al (2017) Dynamic multinuclear sites formed by mobilized copper ions in NO_3 selective catalytic reduction. Science 357(6354):898–903. https://doi.org/10.1126/science.aan5630
10. Paolucci C, Parekh AA, Khurana I, Di Iorio JR, Li H, Albarracin Caballero JD, Shih AJ, Anggara T, Delgass WN, Miller JT et al (2016) Catalysis in a cage: condition-dependent speciation and dynamics of exchanged Cu cations in SSZ-13 zeolites. J Am Chem Soc 138(18):6028–6048. https://doi.org/10.1021/jacs.6b02651
11. Paolucci C, Di Iorio JR, Schneider WF, Gounder R (2020) Solvation and mobilization of copper active sites in zeolites by ammonia: consequences for the catalytic reduction of nitrogen oxides. Acc Chem Res 53(9):1881–1892. https://doi.org/10.1021/acs.accounts.0c00328
12. Chen L, Falsig H, Janssens TVW, Grönbeck H (2018) Activation of oxygen on $(NH_3\text{-Cu-}NH_3)^+$ in NH_3-SCR over Cu-CHA. J Catal 358:179–186. https://doi.org/10.1016/j.jcat.2017.12.009
13. Negri C, Selleri T, Borfecchia E, Martini A, Lomachenko KA, Janssens TVW, Cutini M, Bordiga S, Berlier G (2020) Structure and reactivity of oxygen-bridged diamino dicopper(II) complexes in Cu-ion-exchanged Chabazite catalyst for NH_3-mediated selective catalytic reduction. J Am Chem Soc 142(37):15884–15896. https://doi.org/10.1021/jacs.0c06270
14. Solomon EI, Heppner DE, Johnston EM, Ginsbach JW, Cirera J, Qayyum M, Kieber-Emmons MT, Kjaergaard CH, Hadt RG, Tian L (2014) Copper active sites in biology. Chem Rev 114(7):3659–3853. https://doi.org/10.1021/cr400327t
15. Feng Y, Janssens TVW, Vennestrøm PNR, Jansson J, Skoglundh M, Grönbeck H (2021) The role of H^+- and Cu^+-sites for N_2O formation during NH_3-SCR over Cu-CHA. J Phys Chem C 125(8):4595–4601. https://doi.org/10.1021/acs.jpcc.0c11008
16. Kresse G, Hafner J (1993) Ab initio molecular dynamics for open-shell transition metals. Phys Rev B 48(17):13115–13118. https://doi.org/10.1103/PhysRevB.48.13115
17. Kresse G, Hafner J (1994) Ab initio molecular-dynamics simulation of the liquid-metalamorphous-semiconductor transition in germanium. Phys Rev B 49(20):14251–14269. https://doi.org/10.1103/PhysRevB.49.14251
18. Kresse G, Furthmüller J (1996) Efficient iterative schemes for ab initio total-energy calculations using a plane-wave basis set. Phys Rev B 54(16):11169–11186. https://doi.org/10.1103/PhysRevB.54.11169
19. Kresse G, Furthmüller J (1996) Efficiency of ab-initio total energy calculations for metals and semiconductors using a plane-wave basis set. Comput Mater Sci 6(1):15–50. https://doi.org/10.1016/0927-0256(96)00008-0
20. Perdew JP, Burke K, Ernzerhof M (1996) Generalized gradient approximation made simple. Phys Rev Lett 77(18):3865–3868. https://doi.org/10.1103/PhysRevLett.77.3865
21. Isseroff LY, Carter EA (2012) Importance of reference hamiltonians containing exact exchange for accurate one-shot GW calculations of Cu_2O. Phys Rev B **85**(23), 1–7 (2012). https://doi.org/10.1103/PhysRevB.85.235142
22. Chen L, Janssens TVW, Grönbeck H (2019) A comparative test of different density functionals for calculations of NH_3-SCR over Cu-Chabazite. Phys Chem Chem Phys 21(21):10923–10930. https://doi.org/10.1039/c9cp01576k
23. Grimme S, Antony J, Ehrlich S, Krieg H (2010) A consistent and accurate ab initio parametrization of density functional dispersion correction (DFT-D) for the 94 elements H-Pu. J Chem Phys 132(15):154104. https://doi.org/10.1063/1.3382344
24. Grimme S, Ehrlich S, Goerigk L (2012) Effect of the damping function in dispersion corrected density functional theory. J Comput Chem 32:1456–1465. https://doi.org/10.1002/jcc
25. Blöchl PE (1994) Projector augmented-wave method. Phys Rev B 50(24):17953–17979. https://doi.org/10.1103/PhysRevB.50.17953
26. Kresse G, Joubert D (1999) From ultrasoft pseudopotentials to the projector augmented-wave method. Phys Rev B 59(3):1758–1775. https://doi.org/10.1103/PhysRevB.59.1758
27. Mills G, Jónsson H, Schenter GK (1995) Reversible work transition state theory: application to dissociative adsorption of hydrogen. Surf Sci 324(2–3):305–337. https://doi.org/10.1016/0039-6028(94)00731-4
28. Henkelman G, Jónsson H (2000) Improved tangent estimate in the nudged elastic band method for finding minimum energy paths and saddle points. J Chem Phys 113(22):9978–9985. https://doi.org/10.1063/1.1323224
29. Nosé S (1984) A unified formulation of the constant temperature molecular dynamics methods. J Chem Phys 81(1):511–519. https://doi.org/10.1063/1.447334
30. Hoover WG (1985) Canonical dynamics: equilibrium phase-space distributions. Phys Rev A 31(3):1695–1697. https://doi.org/10.1103/PhysRevA.31.1695
31. Chen L, Falsig H, Janssens TVW, Jansson J, Skoglundh M, Grönbeck H (2018) Effect of Al-distribution on oxygen activation over Cu-CHA. Catal Sci Technol 8(8):2131–2136. https://doi.org/10.1039/c8cy00083b
32. Lam BMT, Halfen JA, Young VG, Hagadorn JR, Holland PL, Lledós A, Cucurull-Sánchez L, Novoa JJ, Alvarez S, Tolman WB (2000) Ligand macrocycle structural effects on copper-dioxygen reactivity. Inorg Chem 39(18):4059–4072. https://doi.org/10.1021/ic000248p
33. Wang X, Chen L, Vennestrøm PNR, Janssens TVW, Jansson J, Grönbeck H, Skoglundh M (2021) Direct measurement of enthalpy and entropy changes in NH_3 promoted O_2 activation over Cu-CHA at low temperature. ChemCatChem 13(11):2577–2582. https://doi.org/10.1002/cctc.202100253
34. Kurth S, Perdew JP, Blaha P (1999) Molecular and solid-state tests of density functional approximations: LSD, GGAs, and meta-GGAs. Int J Quantum Chem 75(4–5):889–909
35. Olsson L, Wijayanti K, Leistner K, Kumar A, Joshi SY, Kamasamudram K, Currier NW, Yezerets A (2015) A multi-site kinetic model for NH_3-SCR over Cu/SSZ-13. Appl Catal B 174:212–224. https://doi.org/10.1016/j.apcatb.2015.02.037